Journal Article

Design and analysis of integrated motor drive for cordless vacuum cleaners

Dianov, A., Sun, X., Xiang, J., and Vagapov, Y.

Design and Analysis of Integrated Motor Drive for Cordless Vacuum Cleaners

Anton Dianov, *Senior Member, IEEE*, Xiaodong Sun, *Senior Member, IEEE*, Jiawei Xiang, *Senior Member, IEEE* and Yuriy Vagapov, *Member, IEEE*

Abstract- **This paper presents the design, development, and experimental evaluation of a high-speed integrated motor drive for cordless vacuum cleaners. The drive employs an axial integration structure, where the inverter PCB is soldered directly to the motor terminals, reducing wiring losses and improving electromagnetic compatibility. A novel PMSM with a star-shaped stator and toroidal winding provides high power density, reduced weight, and enhanced cooling. The motor operates at 120,000rpm, generating airflow enabling forced-air cooling of both the motor and the inverter. The inverter design is constrained by strict geometric and thermal requirements. Its layout is based on the symmetric positioning of six MOSFETs around the motor axis, achieving uniform airflow distribution and reducing local overheating. Experimental tests under variable suction and airflow conditions, simulating realistic VC operation, demonstrated improved thermal management compared with existing commercial solutions, confirming the effectiveness of the proposed integrated drive.**

***Index Terms*—Integrated drives, High speed motors, Permanent magnet motors, Brushless machines.**

I. INTRODUCTION

Recent advances in battery technology have significantly accelerated the development and implementation of autonomous [1] and cordless devices for transportation [2, 3], industrial and domestic applications [4, 5]. It is evident that the leading manufacturers of home appliances are actively investing in research and development to introduce innovative products, with a focus on capturing a larger share of the global market for such devices. In line with this trend, cordless vacuum cleaners (VC) are becoming highly popular worldwide among home users and increasingly dominant in the US and European markets [6]. Despite the higher price compared to wired VCs, about 85% of all vacuum cleaners sold in the US and European markets are now cordless models [7], with the market value predicted to reach $20 billion by 2030 [8]. This strong demand for cordless VCs has driven substantial efforts to develop and manufacture devices with reduced weight and size, increased power density, enhanced efficiency and improved convenience for consumers [9].

The operational performance of VCs is primarily determined by the capabilities of the electric motor applied to generate suction power at the airflow intake [10]. Conventional wired VCs commonly use universal motors [11], whereas cordless VCs are predominantly equipped with permanent magnet synchronous motors (PMSMs) [12], which operate under field-oriented control (FOC) algorithms [13]. Due to the reduced size and weight usually required for cordless appliances, these motors have a compact form factor and significantly increased power density [14]. Obviously, small-sized devices accommodate impellers of lower diameter requiring an increased motor speed to deliver the demanded suction power. Such advanced suction performance is achieved through high-speed motor operation, with the impeller shaft rotating at speeds exceeding 100,000 rpm [15].

A typical PMSM for cordless VCs has a diameter of only a few centimeters but is capable of delivering a rated power of 500-600 W on the shaft while drawing a phase current of 40-50 A. To achieve the required high-speed shaft rotation, the motor typically operates at an AC voltage with a frequency exceeding 2.0 kHz [16]. The high current and frequency significantly contribute to copper and iron losses in the motor, increasing its temperature [17]. Therefore, the combination of compact size and high power density can lead to excessive motor heating, demanding the introduction of efficient cooling methods to ensure safe thermal operation [18, 19].

The standard approach to cooling high-speed motors in VC applications is to arrange the airflow generated by the impeller through the motor [20]. Although the air density varies significantly depending on how the VC is applied during cleaning, this forced air cooling method is considered the simplest, most efficient and cost-effective solution for keeping the motor temperature below the limit [21]. Due to a large volume of air passing through the motor at high speed, heat transfer from the motor surface is highly effective, resulting in a simple design without the need for heatsinks [22, 23].

High-speed motors with small size and low weight, as used in cordless VCs, enable the design and production of compact and lightweight devices [24]. However, the high-speed motors require inverters supplying AC voltage to the stator winding and operating under pulse width modulation (PWM) at frequencies of 20-50 kHz [25], which introduces significant switching losses [26]. To reduce these losses, fast-switching MOSFETs are employed [27], but inverters for high speed motors still experience significant power losses associated with switching time and PWM frequency [28]. At high PWM frequencies, these losses can lead to semiconductor overheating and possible inverter failure [29].

Conduction losses in MOSFETs also contribute substantially to the temperature rise due to the high currents

Anton Dianov is with the Pingyang Institute of Intelligent Manufacturing, Wenzhou University, Wenzhou, 325400, China (e-mail: anton@wzu.edu.cn).

Xiaodong Sun is with the Jiangsu University, Automotive Engineering Research Institute, Zhenjiang, China (e-mail: xdsun@ujs.edu.cn).

Jiawei Xiang is with Wenzhou University, College of Mechanical and Electrical Engineering, Wenzhou, China (jwxiang@wzu.edu.cn).

Yuriy Vagapov is with the Faculty of Arts, Computing and Engineering, Wrexham University, Wrexham, LL11 2AW, UK, (e-mail: yuriy.vagapov@wrexham.ac.uk).

required to supply the stator windings under motor load conditions [30, 31]. In most cordless appliances, including VCs, the battery serving as the power supply is a low-voltage source with a typical value of 24 V. Therefore, in contrast to inverters employed in industrial electric drives and operating at high voltage, the increased current through power semiconductors in VCs results from the relatively low voltage applied at the inverter input [32, 33].

This paper presents a detailed analysis of high-speed integrated electric drives (IEDs) for use in VCs, including thermal management, operational performance, and design approaches. It also proposes a novel high-speed integrated drive for VCs designed to deliver enhanced thermal and operational characteristics. A prototype of the proposed drive was built and tested to validate the design parameters. The main contributions of this paper are as follows:

- ♦ Analysis of integrated motor drives for VCs, including major design challenges and requirements;
- ♦ Analysis and development of a thermal management approach to the design of power inverters in VC IEDs;
- ♦ Proposal of the integrated drive for VC application with enhanced thermal characteristics and operational performance;
- ♦ Experimental validation of the proposed design using a test prototype through a series of practical experiments;
- ♦ Comparative analysis of the proposed integrated motor drive with existing commercial solutions.

II. Advantages and Design Challenges of VC Integrated Drives

Household appliances are designed to meet strict safety and ergonomic standards, which are essential for safe and convenient consumer use [34]. These constraints often make the shape and internal structure of appliances complex for the installation of internal components. Another important factor influencing appliance design is the requirement for low weight [35], which forces designers to use lightweight materials for the appliance enclosure, which complicates the internal structure needed to provide adequate mechanical strength. Such a complex form factor dictates an unconventional approach of enclosing active and passive components, such as batteries, motors, inverters, actuators, cooling systems, and control electronics [36]. This is particularly relevant to cordless VCs, which are often designed for handheld use, where the internal space available for component installation is limited and inconveniently shaped. Complicated design leads to unconventional allocation of components across different areas of the appliance enclosure, often making cooling difficult and, in many cases, nearly impossible [37].

In cordless appliances with complex-shaped enclosures, the motor and inverter are often installed in separate areas and connected by cable wiring. While this configuration is dictated by shape, space, and ergonomic requirements, it can introduce electrical problems, particularly when the inverter operates at high PWM frequencies, employing fast switching semiconductors [38]. Fast switching time generates a high voltage derivative (dv/dt), which may lead to the formation of both direct and reflected voltage waves along the connecting cable in the case of an impedance mismatch between the motor input and the cables [39]. When the cable length is relatively long, the interaction of these waves can result in transient overvoltages at the motor terminals, producing electrical stress on the motor windings and potentially degrading the wire insulation [40]. Additionally, longer cables have increased resistive power losses due to the higher currents in the wires generated by the low voltage power supplies typically used in cordless devices.

The issues discussed above can be solved by integrating the motor, inverter and controller into a single unit, commonly referred to as an integrated electric drive [41]. The compact form factor of the IED enables design optimization, supporting the development of a drive system with improved size and weight characteristics, making easy installation into an appliance enclosure and simplifying overall device assembly [42]. The design and implementation of an IED are particularly important for cordless appliances, especially VCs, where a forced air cooling mechanism is dominant and efficient, effectively supporting the thermal management of electrical and electronic components [44, 43]. In cordless VCs, the appropriate design can enhance the cooling of all the heat-generating components using the high-speed and large volume airflow produced by the motor impeller [45].

An integrated electric drive, in which the inverter is mounted on the motor and connected directly to the motor terminals, provides significant improvement in electromagnetic compatibility, as there are no cable wires between the motor and inverter [46-48]. This direct and short wire connection eliminates impedance mismatch and power loss problems [49]. This solution is particularly important in the design of cordless VC integrated drives, which are powered by a low-voltage battery and carry significant current through the inverter and stator windings [50-52]. Although high currents require costly connectors, switching related overvoltage at the motor terminals and power losses in the connection wires are negligible [53]. Another common connection option is soldering the motor terminal directly to the inverter PCB. This is a cost-effective solution providing significant benefits for mass production.

The air-forced cooling method is widely used in integrated electric drives [54]. It is considered a simple, economical, and efficient approach to the thermal management of all parts comprising the IED [55, 56], which makes this method well suited for use in domestic appliances, including VCs. A typical cooling solution for integrated electric drives is to install the inverter PCB within the motor housing to arrange a common air-forced cooling channel for both the motor and the power semiconductors [57]. In such designs, the motor stator housing is often used as a heat sink for inverter semiconductors [58]. However, the cooling efficiency of these solutions depends significantly on the air speed and airflow volume generated by the rotating components of the motor [59]. Various approaches have been developed to enhance

thermal management in IEDs. For example, [60] proposed to modify the inverter PCB by adding multiple holes to improve air circulation and heat transfer. In cases where airflow is not sufficient for cooling, embedding of semiconductor heat sinks in the motor housing has been suggested by [61] to ensure appropriate thermal management of the inverter.

In IEDs for VCs, enhancing air-forced cooling for semiconductor components is primarily achieved through the proper arrangement of airflow across the inverter PCB, which is typically mounted at the end of the motor. The large airflow volume and high air speed provide operation of the inverter power semiconductors without dedicated heat sinks. However, to ensure efficient heat transfer and reliable thermal management, a thorough design of both the air channel and the PCB configuration of the inverter is essential [62, 63].

Thus, this enhanced air forced cooling approach reduces the overall cost of the motor drive in terms of both assembling and maintenance, while also minimizing size, volume and weight of the device. These factors are particularly important for cordless handheld appliances, as they directly affect usability, ergonomic characteristics and operational performance. Therefore, efficient thermal management is a major design objective in the development of an IED for VCs.

III. Competitive VC Drive

The previously discussed advantage of enhanced cooling in the integrated drives for various fan applications is widely utilized by the manufacturers of home appliances. Typical examples of such drives are demonstrated in Fig. 1, where Fig. 1a illustrates the inverter board of a vacuum cleaner produced by LG Electronics, and Fig. 1b taken from [64] shows the integrated motor drive of a hand dryer developed by Dyson. The solution from LG employs MOSFETs in TO-218 packages, which are relatively tall and significantly obstruct airflow. Furthermore, these components are not rigidly fixed to the PCB, which makes them susceptible to vibrations and reduces overall reliability [65]. The integrated motor drive from Dyson also uses transistors in similar packages, mounted on reduced heatsinks. While this solution demonstrates improved mechanical stiffness and better cooling capability, the metal ribs used as heatsinks occupy additional space, restrict airflow and increase the total cost of the device.

An example of an integrated motor drive produced by Samsung Electronics is demonstrated in Fig. 2, where Fig. 2a illustrates the assembled device, Fig. 2b shows the top side of the inverter PCB corresponding to the motor facing view, and Fig. 2c presents the opposite side of the inverter PCB. This motor drive was obtained from a disassembled cordless VC purchased on the market and is considered a close example of a similar form factor. It will be evaluated in the experimental section and used as a reference in comparative analysis.

In the Samsung integrated drive, the impeller, mounted on the motor shaft, rotates at speeds of approximately 120,000 rpm to generate the required pressure. This device employs axial integration, where the inverter board is soldered directly to the motor terminals. Power transistors are located on the surface of the motor facing side, allowing direct cooling by the incoming airflow. However, the asymmetrical placement of the motor terminals and inverter switches at varying distances from the motor axis results in uneven cooling, potentially causing local overheating and limiting inverter performance. This negative effect is evaluated and analyzed in the experimental section.

Unfortunately, detailed information on the Samsung VC motor drive is proprietary, and the number of available

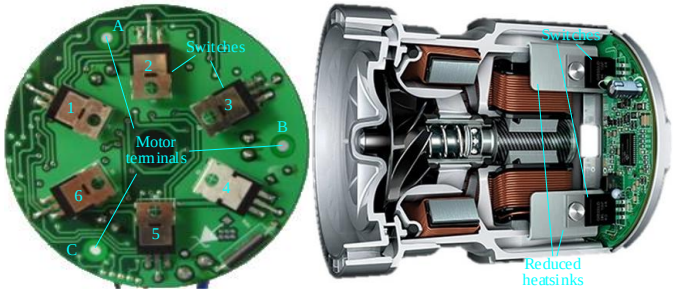

a) b)

Fig. 1. Competitive integrated motor drives: a) VC motor drive from LG; b) Hand dryer motor drive from Dyson, taken from [64].

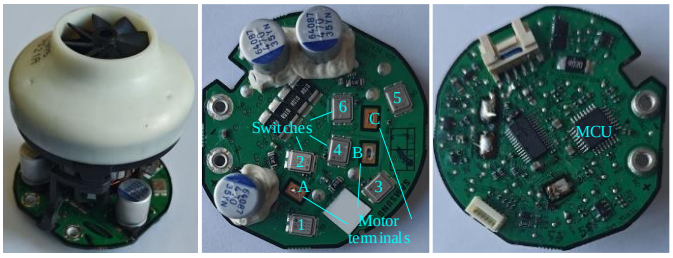

a) b) c)

Fig. 2. Integrated VC motor drive from Samsung Electronics: a) Assembled drive; b) Inverter (motor side view); c) Inverter (outer side view).

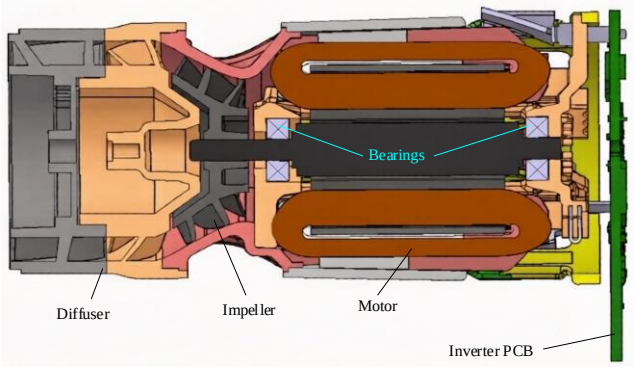

Fig. 3. Construction of the proposed VC motor drive.

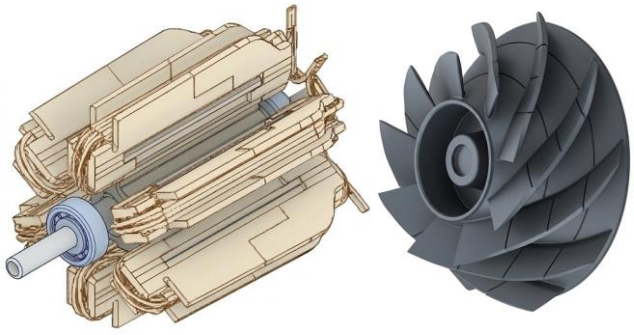

a) b)

Fig. 4. Parts of the proposed VC motor drive: a) Stator and rotor; b) Fan.

publications on this drive is limited. However, some details on the motor drive design and operational performance, have been reported in [66, 67]. Additionally, the motor thermal characteristics based on experimental studies are presented in [68]. Other performance data for this competing device were obtained through testing of a commercially purchased sample.

IV. Proposed Design of Integrated VC Drive

This section describes the construction process of the integrated VC motor drive, including key constraints, inverter component selection, and the development of application-specific control algorithms.

A. Construction of Integrated VC Drive

The proposed design implements a conventional axial integration scheme, as shown in Fig. 3. The inverter PCB is soldered directly to the motor terminals, eliminating excessive wiring. The impeller fan is mounted on the motor shaft, while the impeller housing is fixed to the motor casing. The diffuser, comprising two plastic parts, is attached to the impeller housing. This assembly, referred to as the integrated VC motor drive, is manufactured as a single unit. When the drive is installed in the VC, it can be extended with a fine dust filter, which is tightly mounted to the diffuser.

The impeller is driven by a PMSM, offering high torque-to-weight [69] and torque-to-size [70] ratios along with high efficiency [71] compared to other motor type. Unlike conventional tooth-coil PMSMs [72], the proposed motor uses a novel star-shaped stator with toroidal windings, which improves cooling and enables higher current density and efficiency [73]. The stator and rotor with bearings are shown in Fig. 4a, while the fan designed and validated using the initial prototypes of the motor drive is shown in Fig. 4b. The motor design and its main characteristics are detailed in [73], while its parameters are summarized in Table I.

B. PCB Design Constraints

The PCB design begins with analyzing geometric constraints from the motor and vacuum cleaner, determined by the mechanical engineers who designed the VC handle stick. They define the board shape, mounting holes, and connector positions, thus, appropriate selection and placement of bulky components, such as electrolytic capacitors, is a challenging task, where numerous constraints must be considered [74].

The resulting constraints for the inverter board are shown in Fig. 5a and b for the motor facing and opposite sides, respectively. Bulky components on the motor side may only be placed between motor ribs, with a maximum height of 30 mm, provided that the components' cross-section area occupies less than 50% of the corresponding sector. The height of other components on this side should not exceed 3 mm. On the opposite side of the inverter PCB, components must not exceed 12 mm in height if placed within the designated area; otherwise, their height is limited to 3 mm.

The motor connector consists of three metal pins securely fixed in the motor housing. It must be soldered to the PCB to ensure both the electrical conductivity for current and the mechanical stiffness of the integration. The power connector can be implemented as metal caps fixed at the ends of the

TABLE I. Motor Parameters

Parameter	Value	Parameter	Value
Slot/poles	6/2	Stator resistance, mΩ	40
Rated power, W	860	Direct inductance, μH	7.8
Rated battery voltage, V	25.2	Quadrature inductance, μH	15
Rated phase current, A	50	Back-EMF gain, V/rad/s	0.00085

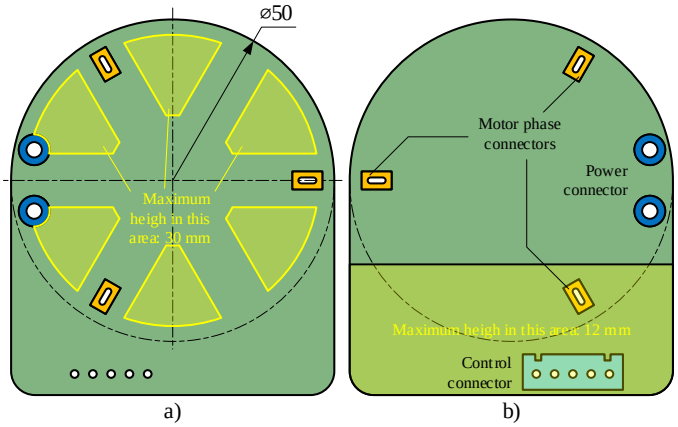

Fig. 5. PCB constraints: a) Motor side; b) opposite side.

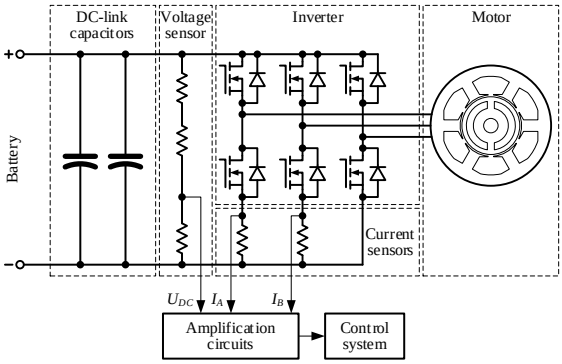

Fig. 6. Inverter schematics.

Fig. 7. Design of inverter PCB.

power supply wires and soldered to the designated holes. Direct soldering of the wires without caps is also possible, however, this option requires verification by reliability engineers. The control connector is preselected by system engineers, may not be changed, and must be located within the designated area on the opposite side of the inverter PCB.

C. Inverter Schematics

After analysis of the requirements, the conventional schematics depicted in Fig. 6 was selected. Since the battery in cordless VCs is located close to the inverter, the EMI filter was omitted from the inverter. DC-link capacitors are included to reduce supply current ripples and stabilize the voltage.

Considering that VC motor drives do not operate at low frequencies, the control algorithm does not require the derivation of a precise motor model. Therefore, the sensor configuration was selected similarly to that used in the majority of low-cost appliances. To measure motor phase currents, the inverter circuit incorporates two shunts located in the bottom legs of the inverter, while the DC-link voltage is measured using a resistive voltage sensor.

D. Selection of Key Parts

The most critical design decision affecting the performance of the integrated motor drive is the selection of inverter semiconductor switches. Analysis of the design constraints and cooling solutions used in competitive drive inverters shows that the transistors should be implemented in low-profile packages. For example, if the cooling approach used in the Dyson motor drive (Fig. 1b) were applied to the proposed motor drive, six plate heatsinks would be required, corresponding to the number of semiconductor switches. Such an inverter design would increase the size of the enclosure, complicate PCB assembly, and reduce device efficiency due to increased resistance airflow during cooling. For this reason, the inverter does not employ dedicated heatsinks. Consequently, minimizing power loss and ensuring sufficient cooling of the switches are extremely important [75]. Therefore, the switches should have low drain-source on-state resistance and low thermal resistance. Based on a detailed analysis, the STL110N10F from STMicroelectronics have been selected. This N-channel Power MOSFET utilizes STripFET F7 technology with an enhanced trench gate structure. It can withstand voltages up to 100 V and can commutate currents of up to 107 A. It has one of the lowest drain-source on-state resistances ($R_{DS(on)}$ = 5 mΩ) combined with low temperature resistances: junction-case resistance $R_{thj\text{-}case}$ = 1.1 °C/W and junction-PCB resistance $R_{thj\text{-}pcb}$ = 31.3 °C/W. The device is implemented in a 5×6 mm PowerFlat package with a height of 1 mm.

The required value of the DC-link capacitor was calculated based on the considerations provided in [76, 77], which analyze the maximum inverter load and maximum allowable ripples of the DC-link voltage. The calculated capacitance of approximately 900 µF could not be implemented as a single component due to the abovementioned geometrical constraints. Therefore, it was achieved using three capacitors rated at 330 µF each, with a maximum height of 16 mm and a diameter of 7 mm, which fully satisfy the design requirements.

To implement reliable current sensing, the metal strip shunt resistors from Vishay with a 1% tolerance were selected. They demonstrate a relatively stable temperature coefficient of resistivity (TCR) [94] and high immunity to electromagnetic noises [78]. To obtain the target resistance of 2 mΩ while improving power dissipation and reducing fault probability, two 4 mΩ resistors were connected in parallel [80].

Due to limited PCB space, high-integration chips capable of implementing multiple circuits are essential. The STSPIN32G4 from STMicroelectronics was selected as the core. It is based on the 170 MHz STM32G4 microcontroller unit (MCU) with motor-control peripherals [81]. However, the main advantage of STSPIN32G4 is the integration of various auxiliary circuits required for inverter applications. It supports 5.5 ~ 75 V supply, includes a low dropout regulator for the MCU circuits, an additional 200 mA buck converter to supply external chips and a triple half-bridge gate driver with bootstrap diodes. The device also provides hardware protection against short circuits, over/under-voltage, and prevents simultaneous conduction of high- and low-side switches in the same inverter leg.

E. Design of Inverter Unit

In the first step, bulky components, such as electrolytic capacitors and the control connector, were arranged according to the constraints in Fig. 5. Airflow analysis for cooling the power semiconductors is challenging due to variations in velocity and complex channel geometry, so finite element analysis (FEA) simulations were conducted. These identified PCB areas with maximal airflow, used to place MOSFETs for efficient, uniform cooling and minimal power-line length.

Semiconductor switches were arranged in pairs near the motor terminals for each phase, equidistant from the motor axis to ensure uniform cooling. The shunt resistors were placed close to the switches, minimizing line length and leveraging impeller airflow. Afterwards, the remaining components were arranged on the PCB, and the final design was validated using 3D design software, Fig. 7. Focusing on cost minimization and considering high integration of inverter circuits, a two layered PCB was selected. Then, the inverter board was carefully routed following the guidelines provided in [82, 83], with particular attention to the routing of sensing elements and analog signal traces.

V. CONTROL SYSTEM

This section discusses the control system of the developed integrated motor drive for VC, focusing on the algorithms specific to the designed device.

A. The Core Control Algorithm

The developing VC motor drive is not intended for operation at low speeds, where the suction power is negligible. Therefore, sensorless algorithms are well suited to the control requirements [84]. The control system used to operate the

developing motor drive is demonstrated in Fig. 8. It employs a back-EMF-based estimator in the *dq* reference frame proposed by Matsui et al. [85]; however, the original approach is enhanced with a speed correction mechanism, which improves response time and performance at higher speeds [86]. To further reduce the reaction time, the control tasks are optimized to update PWM commands within a half period after signal digitalization, mitigating quantization effects and reducing control delays [87, 88]. To reduce the errors caused by the motor rotation during the sampling period, the calculated commands are corrected considering this rotation [89]. The motor drive is started using an open-loop approach with immediate seamless transition to closed-loop control, as proposed in [90]. Open-loop control was found to be unsuitable for stable operation of the VC drive under airflow variations caused by airflow acceleration at startup and occasional blockages of the intake by various debris such as clothes, paper, etc. For this reason, the transition to closed-loop control should occur as soon as the estimator begins operating in the normal mode. The lowest speed at which the estimator starts operating normally is 6,000 rpm, which is therefore selected as the threshold speed for switching from open-loop to closed-loop control.

The modified estimator is equipped with an incremental

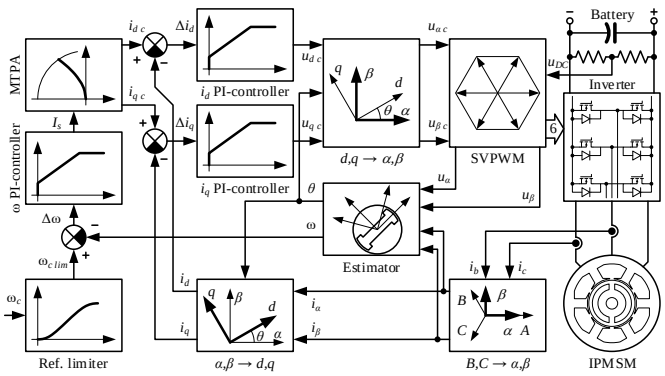

Fig. 8. Control scheme of the VC motor drive (6/2 slot/pole configuration).

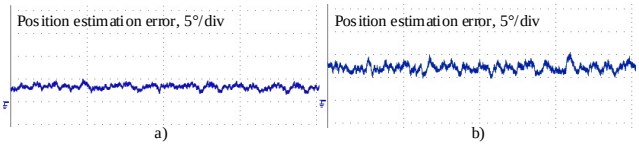

Fig. 9. Estimator errors at 2% load: a) 10,000 rpm; b) 6,000 rpm

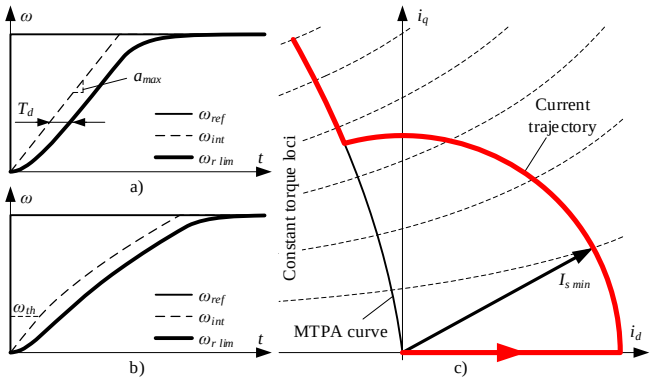

Fig. 10. Operation of system specific algorithms: a) Conventional reference limiter; b) Improved reference limiter; c) Minimum current limitation.

position encoder, whose signals were processed as recommended in [91, 92]. At low speeds, the low back EMF significantly affects the accuracy of position estimation. However, evaluation of the estimator performance shows that the position error at 10,000 rpm is below 5 electrical degrees, as illustrated in Fig. 9a. This speed provides excellent position accuracy and is therefore selected as the minimum speed for stable operation of the control system. At 6,000rpm, when the control transitions from open-loop to closed-loop operation, the position error remains below 10 electrical degrees (Fig. 9b), which is considered acceptable.

The challenges in estimator performance at high (rated) speed are mainly related to the low computational-to-fundamental ratio (CFR). At the rated speed of 120,000 rpm, the CFR is 12.5. This value is close to the lower limit (approximately 10 according to [87]) required for stable FOC, but it does not fall below it. Due to code optimization, the PWM duty cycle is updated at half of the PWM period, which reduces the effective delay to half of the sampling period and results in a delay of only 14.4 electrical degrees. This value is typical for many industrial and household appliance drives and can be easily compensated using corresponding correction in reverse Clarke transformation.

The developed control scheme is based on the conventional FOC topology, comprising an outer speed loop and two inner current loops in the *dq* reference frame. These control loops use PI-controllers, implemented as suggested in [93, 94]. The basic FOC is further enhanced with algorithms to improve the efficiency and performance of the motor drive. The algorithms include maximum torque per ampere control (MTPA), which adapts to variation of motor parameters, as reported in [95]. A field-weakening (FW) algorithm, typically used for operation with discharged batteries [96], was not implemented in the drive control strategy because it significantly increases power loss and complicates cooling. Instead of the FW algorithm, a slight constant reduction of rotor flux was applied to ensure reliable operation of the drive under reduced supply voltage conditions. This flux reduction was achieved through the use of weaker permanent magnets.

The PWM frequency was selected as a tradeoff between control quality and minimization of commutation losses. Based on experimental evaluation, it was set to 25 kHz, corresponding to a sampling time of 40 μs.

B. Specifics of the Compressor Drive

The main specific characteristic of the VC motor drive is its load, which varies quadratically with rotational speed. This behavior introduces non-linear disturbance and requires the implementation of correction techniques, which adjust system gains according to operating speed [97]. The most important blocks requiring gain correction are the speed reference limiter [98, 99] and the current PI-controllers [100, 101].

The operation of a conventional S-shaped reference limiter is illustrated in Fig. 10a. The speed reference limiter receives a step command ω_{ref}, which is initially constrained by the maximum allowable acceleration a_{max}. This limitation

generates an integrated signal ω_{int}, which is further processed through a lowpass filter with a time constant T_d. The resulting S-shaped signal $\omega_{r\,lim}$, is then sent to the speed controller. However, this smooth linear curve leads to a quadratically increased load, which can degrade system performance.

To solve the abovementioned issue, the developed motor drive implements the following algorithm. When the commanded speed exceeds the threshold value ω_{th}, the maximum allowed acceleration a_{max} is reduced proportionally to motor speed. The operation of this technique is demonstrated in Fig. 10b. While this method slightly increases the transient response time, it effectively linearizes the load.

The VC motor's quadratic load complicates low-speed current control, as current is much lower than rated, resulting in a low signal-to-noise ratio. This problem is exacerbated by offset errors in the sensing circuits and accumulating error in the third phase, without dedicated shunt [102]. Therefore, conventional control can distort readings, degrading performance [103] and trigger overcurrent faults. To address this, the proposed algorithm limits the minimum stator current amplitude to maintain reliable sensing, while adjusting the current vector phase to produce the required torque. It is illustrated in Fig. 10c, showing the modified current trajectory.

C. Safety Issues

Household appliances must ensure safe and reliable operation, as regulated by UL60730 standard [104]. The STSPIN32G4 motor controller provides hardware protections, including overtemperature and abnormal voltage detection, and monitors each transistor's drain-source voltage. Therefore, some critical protections are implemented in hardware, simplifying development. Hardware protections are complemented by software protections for overvoltage [105] and phase loss failures [106]. Without a heatsink, insufficient airflow can rapidly overheat inverter switches, so NTCs are placed between transistors in each inverter leg, monitoring two devices simultaneously to save space and cost.

The developing system also includes self-testing routines for UL60730 Class B compliance, eliminating external protective devices. It reduces both cost and size of the VC, which is crucial for the competitive home appliance market.

VI. Experimental Investigation

This section discusses the equipment used in this research, outlines its characteristics and explains the testing approaches. It also details the test procedures, presents the experimental data, and provides its comparative analysis.

A. Experimental Equipment

A test prototype of the proposed electric drive was produced and tested to evaluate its performance. The prototype with a detached inverter is shown in Fig. 11a, while both sides of the inverter PCB are presented in Fig. 11b and c.

Fig. 12 demonstrates test setup for developing control software and evaluating motor signals. To study airflow performance, a dedicated test rig, capable of controlling motor-drive airflow and simulating various VC operating modes, was constructed, Fig. 13a. The rig includes a manometer box coupled with the testing motor drive using a special airflow connector, shown in Fig. 13b (opened) and Fig. 13c (closed). This box includes an orifice control unit in the form of a pipe with a hermetic clamp designed to hold interchangeable circular metal orifices of different diameters to regulate airflow and simulate different loads.

Inverter switch temperatures were measured with thermocouples and recorded using a Yokogawa FX1000, while voltage and current were captured with a Yokogawa DL-850 oscilloscope. The motor drive was powered by a

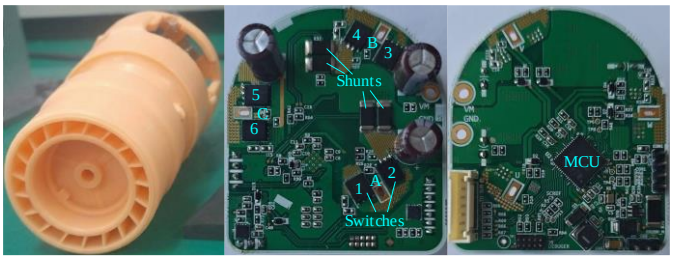

a) b) c)

Fig. 11. Test rig for motor signals evaluation: a) Motor with impeller and diffuser; b) Inverter (motor side view); c) Inverter (outer side view).

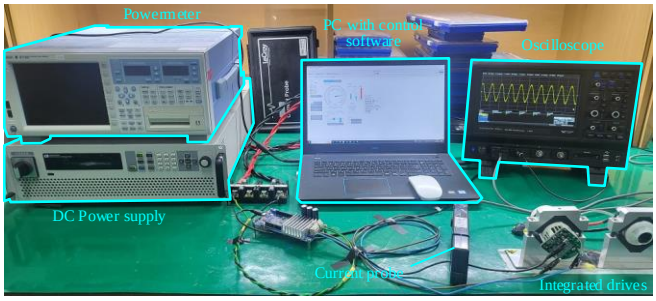

Fig. 12. Test rig for motor signals evaluation.

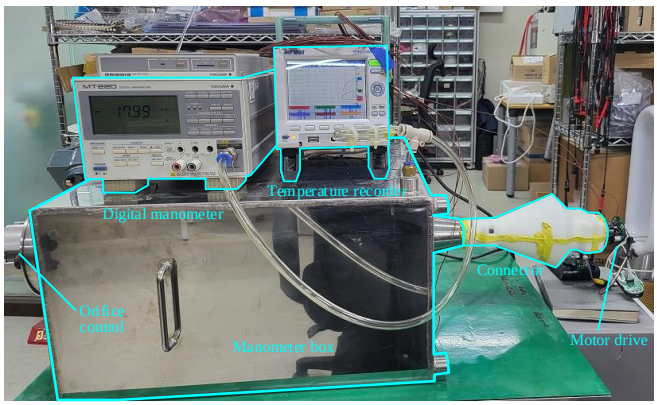

a)

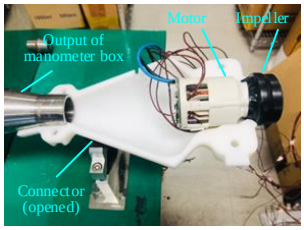

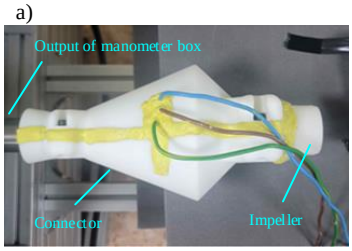

b) c)

Fig. 13. Test rig for VC motor drive evaluation. a) Equipment; b) Opened connector; c) Motor with impeller, connected to the manometer box.

Techways Kewell C3000H (up to 3 kW DC) and controlled via PC through a USB for automated data acquisition.

The developed VC drive was tested under various speeds and operational modes using the developed control system. For a fair comparison, the competitive device was tested using its native inverter and control, therefore the number of its operational modes was limited to "Min", "Med" and "Max".

Safety requirements dictated that transistor case temperature remain below 115 °C to ensure the stiffness and mechanical integrity of the plastic parts. With a maximum ambient of 50 °C, it gives a 65°C of allowable temperature rise. Since all experiments were conducted at 24 °C and standard atmospheric pressure, the maximum permissible temperature for inverter switches in the tests was 89 °C.

B. Experimental Results

The first series of experiments evaluated the control system with modified blocks. Under conventional control, very low load torque produces low motor current, thus sensing noise heavily distorts the waveform, risking overcurrent faults, Fig. 14a. Introducing a minimum current limit of 1 A improves the waveform, Fig. 14b. The conventional S-shaped limiter causes a parabolic current increase due to the quadratic fan load, Fig. 15a. After modifying the block and adjusting its gain based on motor speed, the system load was effectively linearized, Fig. 15b.

The next series of experiments compares the power-speed characteristics of the proposed and Samsung drives. The results of these experiments are shown in Fig. 16, which demonstrates that the developed prototype outperforms the Samsung drive, achieving higher rotational speeds and power.

Thermal behavior of the inverter switches was evaluated under varying suction conditions, simulating changes in airflow caused by application, dust level, or debris. Airflow was regulated using circular orifices of 5, 8, 10, 12, 16, 24 mm diameter, representing fully blocked to fully open inlets, with intermediate sizes simulating partial blockage. It should be noted, however, that even under fully blocked conditions, airflow is not completely stopped, as leakage occurs through gaps in the VC housing and piping.

In the first test, the temperature rise of inverter switches

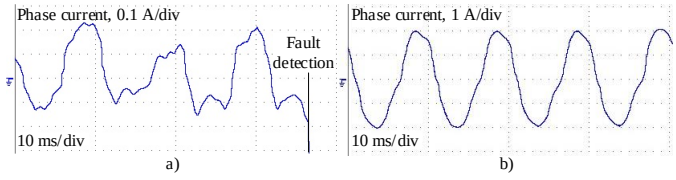

Fig. 14. Operation at low load at 6000 rpm: a) Conventional; b) Improved

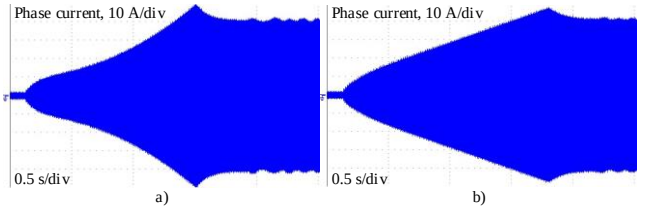

Fig. 15. Motor phase current at speed increase from 6,000 to 120,000 rpm. a) With S-shaped reference limiter; b) With improved reference limiter

for two drives was analyzed for the rated conditions. Motor drives operated at its maximum speed n and with an orifice of a maximum diameter $\varnothing_{or} = 24$ mm. The results are shown in Fig. 17a and b for Samsung and test drives, respectively. It is shown that the transistors in Samsung drive heat unevenly with a temperature difference of approximately 8 °C, while the

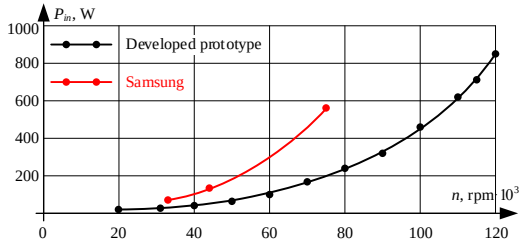

Fig. 16. Power-speed characteristics of VC motor drives.

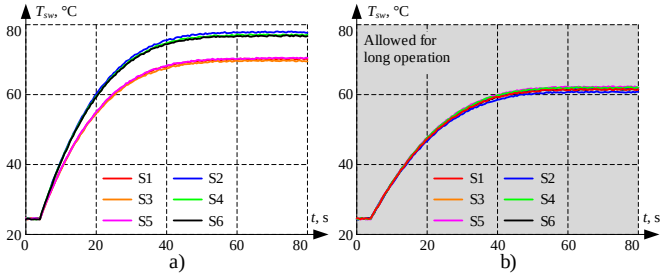

Fig. 17. Temperature rising test with $\varnothing_{or} = 24$ mm: a) Samsung VC drive at $n = 76$ krpm; b) Developed VC drive at $n = 120$ krpm

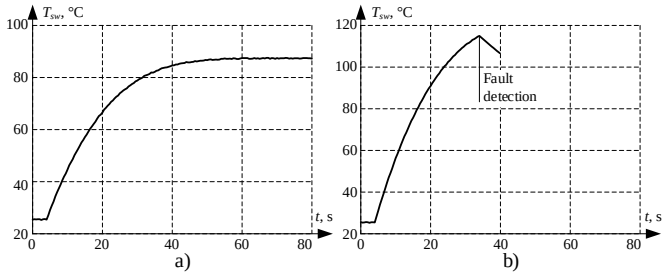

Fig. 18. Temperature rising test of Samsung VC drive at $n = 76$ krpm: a) $\varnothing_{or} = 16$ mm; b) $\varnothing_{or} = 5$ mm

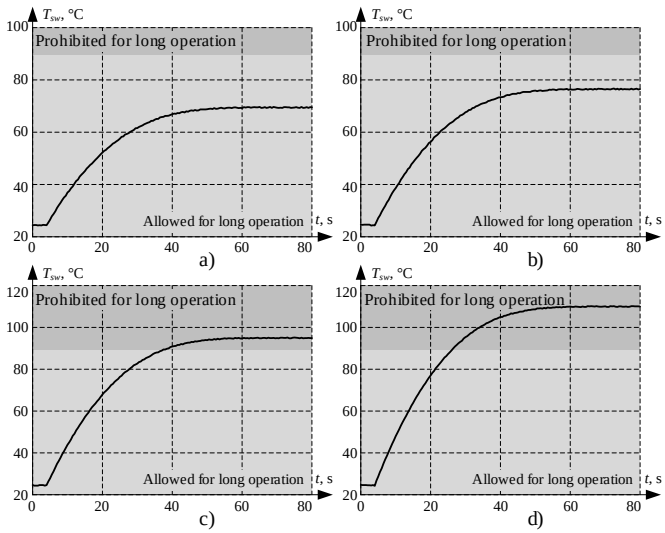

Fig. 19. Temperature rising test of developed VC drive at $n = 120$ krpm: a) $\varnothing_{or} = 16$ mm; b) $\varnothing_{or} = 12$ mm; c) $\varnothing_{or} = 8$ mm; d) $\varnothing_{or} = 5$ mm

proposed drive switches heat uniformly with a temperature difference of approximately 1.5 °C. The highest temperature among switches was observed at transistor #2 in the Samsung drive and transistor #5 in the developed drive. Therefore, they may be used as a representative of the maximum temperatures.

The next thermal test evaluated the Samsung drive under two load conditions using 16 and 5 mm orifices. The results of the test are shown in Fig. 18a and b. The 16 mm orifice raised inverter temperature to 87 °C, while the 5 mm orifice triggered fault detection after approximately 30 s of operation.

The final test examined the developed drive at maximum speed with 16, 12, 8, and 5 mm orifices. The test results are shown in Fig. 19a, b, c and d, respectively. It can be observed that the inverter temperature exceeds the limit only with 5mm and 8 mm orifices; however, thermal protection is not activated due to the relatively lower ambient temperature.

VII. Discussion

The primary advantage of the proposed integrated motor drive is its enhanced cooling, enabling higher rated power and greater suction in a compact form factor. Symmetrical placement of inverter switches ensures uniform cooling, reducing operating temperatures and extending lifespan. Unlike reference designs with asymmetrical layouts that rely on costly metal-case transistors, the proposed layout allows standard plastic-packaged switches, lowering cost without reducing reliability. Compact, high-integration STSPIN32G4 controller decreases PCB space and development time, resulting insignificant increase of VC competitiveness.

VC load strongly depends on the airflow inlet area and decreases as the area shrinks. The most critical thermal condition occurs with a fully blocked inlet: lower airflow reduces motor load but also decreases cooling efficiency, putting the drive and inverter switches at risk of overheating. To prevent damage, operating time under blocked conditions is strictly limited. Thermal safety is typically ensured with either motor thermal protection (less common) or a choke valve (more common), which activates at a preset pressure difference to maintain minimal airflow for cooling.

Thermal tests confirm that the integrated drive operates stably under a wide range of loads, including partially and fully blocked inlets. This improved cooling allows a less sensitive choke valve, reducing interruptions while maintaining safe operation.

Mounting the inverter PCB directly on the motor housing ensures efficient cooling from high-velocity airflow, eliminating the need for heatsinks. Modeling shows a comparable natural-air-cooled PCB would require a 50 cm^3, 135 g aluminum heatsink, so this integration saves about $0.4 per device. Soldering the PCB directly to the motor terminals also removes extra wires and connectors, additionally saving about $0.4. Therefore, this integrated approach improves performance, simplifies assembly, and reduces costs, which is beneficial for mass production.

VIII. Conclusions

This study presents the design, development, and experimental validation of a high-speed integrated motor drive for cordless VC. Using axial integration, the inverter PCB is mounted on the motor rear and soldered directly to the terminals, reducing wiring, losses, and improving EMI. A novel PMSM with a star-shaped stator and toroidal windings delivers high power density and enhanced cooling, rotating the impeller at 120,000 rpm to provide forced-air cooling.

The inverter PCB design follows strict constraints on geometry and by airflow management ensures uniform cooling of 6 MOSFETs, preventing local overheating. A sensorless FOC algorithm with speed correction and MTPA optimization enables efficient operation across varying suction conditions.

Experimental results show the proposed drive outperforms competitive designs in thermal management and efficiency while maintaining a compact size, offering a cost-effective solution for high-performance domestic and industrial VCs.

Acknowledgment

The developed VC motor drive was highly recognized by the Korean government and was awarded the 2023 New Excellent Technology Award by the Ministry of Trade, Industry and Resources of Republic of Korea.

References

[1] V. Prakht, et al., “Analysis of performance improvement of passenger car synchronous homopolar generator with the addition of ferrite magnets”, Appl. Sci., 13, 3990, pp. 1–19, Mar. 2023.

[2] C. Li, W. Huang, R. Cao, F. Bu and C. Fan, “An integrated topology of charger and drive for electric buses,” IEEE Trans. on Veh. Technol., vol. 65, no. 6, pp. 4471-4479, Jun. 2016.

[3] J.A. Swanke and T.M. Jahns, “Reliability analysis of a fault-tolerant integrated modular motor drive for an urban air mobility aircraft using Markov chains,” IEEE Trans. Transp. Electrific., vol. 8, no. 4, pp. 4523-4533, Dec. 2022.

[4] A.A. Khan, D. Afriyie, M. Al Saaideh and S. Ahmed, “A novel and simple integrated on-board charger for E-mobility,” IEEE Trans. Ind. Electron., vol. 72, no. 4, pp. 3534-3542, Apr. 2025

[5] Y. Yang et al., “Model predictive torque control of six-phase switched reluctance motors based on improved voltage vector strategy,” IEEE Trans. Transp. Electrific., vol. 11, no. 3, pp. 7650-7661, Jun. 2025.

[6] Y. Xiao, et al., “Survey data on customer two-stage decision-making process in household vacuum cleaner market,” Data in Brief, vol. 54, Jun. 2024, Art. no. 110353.

[7] Q. Bi and D. Shao, “Loss analysis of high-speed permanent magnet motor for cordless vacuum cleaner,” Journal of Physics: Conference Series, vol. 2488, 2023, Art. no. 012021.

[8] J. Lin, et al., “Performance testing of cordless handheld vacuum cleaners,” Aerosol and Air Quality Research, vol. 24, no. 10, Oct. 2024, Art. no. 240082.

[9] Y. Choo, et al., “Investigation of systematic efficiency in a high-speed single-phase brushless DC motor using multi-physics analysis for a vacuum cleaner,” IEEE Trans. Magn., vol. 55, no. 7, July 2019, Art. no. 8203606.

[10] A. Spampinato, G. Forte, G. Scelba and G. De Donato, “A cost-effective switched reluctance motor drive for vacuum cleaners,” Int. Symp. Power Electron., Elect. Drives, Automat. Motion, 2020, pp. 36-41.

[11] A. Dianov, et al., “Substitution of the universal motor drives with electrolytic capacitorless PMSM drives in home appliances,” Int. Conf. Power Electron. ECCE Asia, 2015, pp. 1631–1637.

[12] G. Zhang et al., “Pseudorandom-frequency sinusoidal injection for position sensorless IPMSM drives considering sample and hold effect,” IEEE Trans. Power Electron., vol. 34, no. 10, pp. 9929-9941, Oct. 2019.

[13] J. Huo, et al., "Torque ripple compensation with anti-overvoltage for electrolytic capacitorless PMSM compressor drives," IEEE J. Emerg. Sel. Topics Power Electron., vol. 10, no. 5, pp. 6148-6159, Oct. 2022.

[14] H. Arita, K. Nishiwaki, M. Iezawa and T. Kosaka, "High speed homopolar type permanent magnet motor designed for fast acceleration response," 23rd Int. Conf. Elect. Mach. Syst., 2020, pp. 1930-1935.

[15] F. Xu, et al., "Influence of slot number on electromagnetic performance of 2-pole high-speed permanent magnet motors with toroidal windings," IEEE Trans. Ind. Appl., vol. 57, no. 6, pp. 6023–6033, Nov.-Dec. 2021.

[16] Z. Lia, P. Wang, L. Liu, Q. Xu, S. Che, L. Zhang, S. Du, H. Zhang, and H. Sun, "Loss calculation and thermal analysis of ultra-high speed permanent magnet motor," Heliyon, vol. 8, 2022, Art. no. e11350.

[17] Z. Cui, et al., "A low rotor eddy current loss design approach to HSPMSM for small-scale magnetically suspended turbomolecular pump," IEEE Trans. Ind. Electron. v. 72, no. 6, pp. 6265-6275, Jun. 2025.

[18] K. Sim, Y.-B. Lee, S.-M. Jang, and T.H. Kim, "Thermal analysis of high-speed permanent magnet motor with cooling flows supported on gas foil bearings: Part I - coupled thermal and loss modelling," J. Mech. Science Tech., vol. 29, no. 12, pp. 5469–5476, 2015.

[19] A. Dianov, J.-W. Kang, "Decreasing noise pollution of the automotive compressor in preheating mode," IEEE Trans. Energy Convers., vol. 40, no. 4, pp. 3093-3103, Dec. 2025.

[20] M. Xu, Z. Qiu, and Z. Wang, "Research on weakening control strategy of permanent magnet synchronous motor of high speed vacuum cleaner based on sliding mode observer," in Proc. Int. Conf. on Computers, Information Processing and Advanced Education, 2023, pp. 562–568.

[21] J. Dong, Y. Huang, L. Jin, H. Lin, and H. Yang, "Thermal optimization of a high-speed permanent magnet motor," IEEE Transactions on Magnetics, vol. 50, no. 2, Feb. 2014, Art. no. 7018504.

[22] K. Hu, G. Zhang, and W. Zhang, "Analysis and optimization of temperature field of high-speed permanent magnet motor," Advances in Mechanical Engineering, vol. 14, no. 5, pp. 1–11, May 2022.

[23] A. Sharp, et al., "A test rig for thermal analysis of heat sinks for power electronic applications," in Proc. IEEE East-West Design & Test Symposium, Batumi, 2023, pp. 1-4.

[24] V. Dmitrievskii, V. Prakht, V. Kazakbaev and S. Sarapulov, "Optimal design of a high-speed single-phase flux reversal motor for vacuum cleaners," Energies, 11, 3334, pp. 1–13, Nov., 2018.

[25] V. Prakht, et al., "High speed flux reversal motor for power tool," 6th Int. Electric Drives Prod. Conf., 2016, pp. 306-311.

[26] A.H. Mohamed, et al., "Electrothermal design of a discrete GaN-based converter for integrated modular motor drives," IEEE J. Emerg. Sel. Topics Power Electron., vol. 9, no. 5, pp. 5390-5406, Oct. 2021.

[27] A.K. Morya et al., "Wide bandgap devices in AC electric drives: opportunities and challenges," IEEE Trans. Transp. Electrific., vol. 5, no. 1, pp. 3-20, Mar. 2019.

[28] Z Li, et al., "Loss analysis of high-speed permanent magnet motor based on energy saving and emission reduction," Energy Reports, vol. 9, pp. 2379–2394, 2023.

[29] G. Rohner, et al., "Comparative evaluation of three-phase three-level GaN and seven-level Si flying capacitor inverters for integrated motor drives considering overload operation," IEEE Access, vol. 12, pp. 7356-7371, 2024.

[30] G. Rohner et al., "Hardware-based comparative analysis of multilevel inverter topologies for integrated motor drives considering overload operation," IEEE Open J. Power Electron., vol. 4, pp. 934-944, 2023.

[31] G.H. Chen, et al., "Research on thermal error compensation modeling for the machine tool integrated drive system based on energy consumption big data and an optimized bidirectional network," Prec. Eng., vol. 94, pp. 91-112, Feb. 2025.

[32] A. Dianov, "An algorithm for offline measurement of motor stator resistance and voltage drop across inverter switches for washing machine drives," IEEE J. Emerg. Sel. Topics Power Electron., vol. 10, no. 5, pp. 5798-5808, Oct. 2022.

[33] S. Saponara, et al., "Design and measurement of integrated converters for belt-driven starter-generator in 48 V micro/mild hybrid vehicles," IEEE Trans. Ind. Appl., vol. 53, no. 4, pp. 3936-3949, Jul./Aug. 2017.

[34] A. Dianov, et al., "Future drives of home appliances: Elimination of the electrolytic DC-link capacitor in electrical drives for home appliances," IEEE Ind. Electron. Mag., vol. 9, no 3, pp. 10–18, Sep. 2015.

[35] M.-S. Lim, J.-M. Kim, Y.-S. Hwang and J.-P. Hong, "Design of an ultra-high-speed permanent-magnet motor for an electric turbocharger considering speed response characteristics," IEEE/ASME Trans. Mechatronics, vol. 22, no. 2, pp. 774-784, April 2017.

[36] M.R. Khowja et al., "Novel permanent magnet synchronous motor with integrated filter inductor, using motor's inherent magnetics," IEEE Trans. Ind. Electron., vol. 68, no. 7, pp. 5638-5649, Jul. 2021.

[37] T.M. Jahns and H. Dai, "The past, present, and future of power electronics integration technology in motor drives," CPSS Trans. Power Electron. Appl., vol. 2, no. 3, pp. 197-216, Sept. 2017.

[38] A. Anuchin, et al., "Increasing Current Loop Performance Using Variable Accuracy Feedback for GaN Inverters," 21st International Symposium on Power Electronics (Ee), 2021, pp. 1-5.

[39] W. Zhou, et al., "Inverter with paralleled modules to extend current capacity and combat motor overvoltage in SiC-based adjustable speed drives," IEEE Trans. Ind. Electron., vol. 71, no. 5, pp. 4474-4484, May 2024.

[40] W. Zhou, X. Yuan and Z. Zhang, "An active dv/dt filter to combat motor terminal overvoltage in SiC-based adjustable speed drives," IEEE Trans. Ind. Electron., vol. 72, no. 1, pp. 1076-1081, Jan. 2025.

[41] S. Chen, M. Hu, "Active torsional vibration suppression of integrated electric drive system based on optimal harmonic current instruction analytic calculation method," Mechanism Mach. Theory, vol.180, pp. 1-24, Jan. 2023.

[42] Z. Sun, et al., "Optimization of electromagnetic vibration for integrated electric drive systems based on electric vehicle driving cycle considering energy consumption," Energy, vol. 313, pp. 1-13, Nov. 2024.

[43] J. Cai, X. Zhang, W. Zhang and Y. Zeng, "An integrated power converter-based brushless DC motor drive system," IEEE Trans. Power Electron., vol. 37, no. 7, pp. 8322-8332, Jul. 2022.

[44] J.W. Lee, et al., "Heat source and internal temperature estimation of an integrated modular motor drive in robotic application using inverse heat conduction problem," Meas., vol. 243, pp. 1-12, Jan. 2025.

[45] N. Bianchi, et al., "Potentials and limits of high-speed PM motors," IEEE Trans. Ind. Appl., vol. 40, no. 6, pp. 1570-1578, Nov.-Dec. 2004.

[46] O. Gulsuna, et al., "Design and analysis of a GaN-based megahertz integrated motor drive for a PCB motor," IEEE Trans. Ind. Electron., vol. 71, no. 12, pp. 15435-15444, Dec. 2024.

[47] T. Payarou and P. Pillay, "Integrated multipurpose power electronics interface for electric vehicles," IEEE Trans. Transp. Electrific., vol. 9, no. 2, pp. 2429-2443, Jun. 2023.

[48] J. Hu, et al., "Optimal energy consumption and torque fluctuation control of integrated electric drive system based on mechanical electromagnetic-thermal coupling characteristics," Energy, vol. 247, pp. 1-14, Feb. 2022.

[49] A. Galassini, et al., "A modular speed-drooped system for high reliability integrated modular motor drives," IEEE Trans. Ind. Appl., vol. 52, no. 4, pp. 3124-3132, Jul./Aug. 2016.

[50] K. B. Jang, Sung Hong Won, Tae Heoung Kim and Ju Lee, "Starting and high-speed driving of single-phase flux-reversal motor for vacuum cleaner," IEEE Trans. Magn., vol. 41, no. 10, pp. 3967-3969, Oct. 2005.

[51] G. Rizzoli, et al., "Torque ripple suppression in three-phase doubly-fed machine for wireless power transfer in integrated drives," IEEE Trans. Ind. Electron., vol. 71, no. 9, pp. 10198-10209, Sep. 2024.

[52] G. Nobile, et al., "Losses minimization control for an integrated multidrive topology devoted to hybrid electric vehicles," IEEE Trans. Ind. Electron., vol. 66, no. 11, pp. 8345-8360, Nov. 2019.

[53] S. Wang and P. W. Lehn, "A three-phase electric vehicle charger integrated with dual-inverter drive," IEEE Trans. Transp. Electrific., vol. 8, no. 1, pp. 82-97, Mar. 2022.

[54] J. Hu, et al., "Study on low-frequency torsional vibration suppression of integrated electric drive system considering nonlinear factors," Energy, vol. 284, pp. 1-16, Oct. 2023.

[55] R. Wrobel "A technology overview of thermal management of integrated motor drives – electrical machines," Thermal Sci. Eng. Prog., vol. 29, pp. 1-14, Feb. 2022.

[56] S.S. Nielsen, R.K. Holm and P.O. Rasmussen, "Conveyor system with a highly integrated permanent magnet gear and motor," IEEE Trans. Ind. Appl., vol. 56, no. 3, pp. 2550-2559, May/Jun. 2020.

[57] R. Amorim Torres, et al., "Current-source inverter integrated motor drives using dual-gate four-quadrant wide-bandgap power switches," IEEE Trans. Ind. Appl., vol. 57, no. 5, pp. 5183-5198, Sep./Oct. 2021.

[58] L. Tang, G.-J. Su and X. Huang, "Experimental high-performance control of two permanent magnet synchronous machines in an integrated drive for automotive applications," IEEE Trans. Power Electron., vol. 23, no. 2, pp. 977-984, Mar. 2008.

[59] W. Lee, et al., "A review of integrated motor drive and wide-bandgap power electronics for high-performance electro-hydrostatic actuators," IEEE Trans. Transp. Electrific., vol. 4, no. 3, pp. 684-693, Sep. 2018.

[60] J. Wang, Y. Li and Y. Han, "Integrated modular motor drive design with GaN power FETs," IEEE Trans. Ind. Appl., vol. 51, no. 4, pp. 3198-3207, Jul./Aug. 2015.
[61] R. Abebe, et al., "Integrated motor drives: state of the art and future trends," IET Electr. Power Appl., vol. 10, n. 8, pp. 757–771, Dec. 2016.
[62] A. Tenconi, F. Profumo, S. E. Bauer and M. D. Hennen, "Temperatures evaluation in an integrated motor drive for traction applications," IEEE Trans. Ind. Electron., vol. 55, no. 10, pp. 3619-3626, Oct. 2008.
[63] M. Haider, P. S. Niklaus, M. Madlener, G. Rohner and J. W. Kolar, "Comparative evaluation of gate driver and LC-filter based dv/dt-limitation for SiC-based motor-integrated variable speed drive inverters," IEEE Open J. Power Electron., vol. 4, pp. 450-462, 2023.
[64] Dyson airblade tap. Online https://www.gr.dyson.com/medialibrary/Commercial_V5/Downloads/Tap%20Range%20Brochures/75360_DYS_AB_RoA_AIRBLADE-TAP-BROCHURE_DIGITAL_VERSION_SEPT-2015.pdf
[65] J. Chen, et al., "Numerical model-aided intelligent diagnosis method to detect faults in induction motors," IEEE Sensors Journal, vol. 25, no. 17, pp. 32194-32208, Sep., 2025
[66] B. Jung, P. Jang, J. Kim, S. Lim and K. Nam, "Intermittent Inductance Estimation for High-Speed PMSM Sensorless Control," 2020 IEEE Applied Power Electronics Conf. Expo., 2020, pp. 248-252.
[67] W. Hwang, J. Kim, J. Han, W. Kang, and S. Park, "Investigation of resonance avoidance method for vacuum cleaner," IEEE Open Journal of Industry Applications, vol. 4, pp. 328–335, 2023.
[68] A. Dianov, X. Sun, G. Demidova, N. Tarlavin and J. Xiang, "Ultra-high-speed motor drive for cordless vacuum cleaner," IEEE Trans. Energy Convers., DOI: 10.1109/TEC.2025.3634130.
[69] K. Li et al., "Compensation control of PMSMs based on a high-order sliding mode observer with inertia identification," IEEE J. Emerg. Sel. Topics Power Electron., vol. 13, no. 4, pp. 5084-5096, Aug. 2025.
[70] A. Lukin, G. Demidova, A. Rassõlkin, D. Lukichev, T. Vaimann and A. Anuchin, "Small magnus wind turbine: modeling approaches," Appl. Sci., 12, 1884, Feb. 2022.
[71] R.C. Bolam, et al., "Prototype testing of rim driven fan technology for high-speed aircraft electrical propulsion," in Proc. Int. Universities Power Eng. Conf., 2024, pp. 1-5,
[72] G. Zhang et al., "Adaptive step-size predictive PLL based rotor position estimation method for sensorless IPMSM drives," IEEE Trans. Power Electron., vol. 39, no. 5, pp. 6136-6147, May 2024.
[73] T.R. He, et al., "Comparison of toroidal and tooth-coil winding 2-pole slotted high-speed permanent magnet motors," IEEE Trans. Ind. Appl., vol. 60, no. 3, pp. 3870–3882, May-Jun. 2024.
[74] A.H. Mohamed, H. Vansompel and P. Sergeant, "Polygon-retrofitted integrated modular motor drive for switched reluctance machines," IEEE Trans. Ind. Electron., vol. 69, no. 12, pp. 12469-12479, Dec. 2022.
[75] A. Sharp, et al., "Numerical optimisation of air-cooled heat sink geometry to improve temperature gradient of power semiconductor modules," in Proc. XV Int. Symp. Ind. Electron. Appl., 2024, pp. 1-6.
[76] A. Safayet, M. Islam and T. Sebastian, "Sizing of DC-link capacitor considering voltage and current ripple requirements for a 3-phase voltage source inverter," IEEE Energy Conv. Congr. Expo., 2020, pp. 1512-1518.
[77] M.N. Anwar and M. Teimor, "An analytical method for selecting DC-link-capacitor of a voltage stiff inverter," IEEE Ind. Appl. Conf., 2002, pp. 803-810.
[78] T. Chen, et al., "Electromagnetic compatibility analysis of an induction motor drive with integrated power converter," IEEE Trans. Magn., vol. 56, no. 1, pp. 1-4, Jan. 2020.
[79] A. Anuchin, et al. "Accuracy analysis of shunt current sensing by means of delta-sigma modulation in electric drives." Int. Ural Conf. on AC Electric Drives, pp. 1–5, 2018.
[80] G. Zhang, H. Zhou, G. Wang, C. Li and D. Xu, "Current sensor fault-tolerant control for encoderless IPMSM drives based on current space vector error reconstruction," IEEE J. Emerg. Sel. Topics Power Electron., vol. 8, no. 4, pp. 3658-3668, Dec. 2020.
[81] A. Lörsch, et al., "Practical learning of DSP-based motor control for engineering students," Int. Universities Power Eng. Conf., 2024, pp. 1-5.
[82] A. Dianov, "Recommendations and typical errors in design of power converter PCBs with shunt sensors," IEEE Open J. of the Ind. Electronics Soc., vol. 3, pp. 329-338, 2022.
[83] A. Dianov et al., "Recommendations and typical errors on usage of wirewound resistors in design of power converters," IEEE Open Journal of the Industrial Electronics Society, vol. 6, pp. 669-684, 2025.
[84] G. Zhang et al., "PR internal mode extended state observer-based iterative learning control for thrust ripple suppression of PMLSM drives," IEEE Trans. Power Electron., vol. 39, no. 8, pp. 10095-10105, Aug. 2024.
[85] N. Matsui, "Sensorless PM Brushless DC Motor Drives", IEEE Trans. Ind. Electron., Vol. 43, No. 2, Apr, 1996, pp. 300-308.
[86] A. Dianov, Y.K. Kim, S.J. Lee, S.T. Lee and T.H. Yoon., "Sensorless IPMSM based drive for reciprocating compressor," in Proc. 13th Int. Power Electron. Motion Control Conf., 2008, pp. 1002–1008.
[87] H.A.A. Awan, T. Tuovinen, S.E. Saarakkala and M. Hinkkanen, "Discrete-time observer design for sensorless synchronous motor drives," IEEE Trans. Ind. Appl., vol. 52, no. 5, pp. 3968-3979, Sept.-Oct. 2016.
[88] T. Li et al., "Model-free predictive control for harmonic suppression of PMSMs based on adaptive resonant controller," IEEE Trans. Energy Conv., vol. 40, no. 4, pp. 3104-3114, Dec. 2025.
[89] B.-H. Bae and S.-K. Sul, "A compensation method for time delay of full-digital synchronous frame current regulator of PWM AC drives," IEEE IEEE Trans. Ind. Appl., vol. 39, no. 3, pp. 802-810, May-June 2003.
[90] A. Dianov, "Instant closing of permanent magnet synchronous motor control systems at open-loop start," Sustainability, 14, 12665, pp. 1–18, Oct., 2022.
[91] A. Anuchin, et al., "Speed estimation algorithm with specified bandwidth for incremental position encoder," In Proc. 2016 17th Int. Conf. on Mechatronics - Mechatronika (ME), pp. 1–6, 2016.
[92] A. Anuchin, et al., "Synchronous constant elapsed time speed estimation using incremental encoders," IEEE/ASME Transactions on Mechatronics, vol. 24, no 4, pp. 1893–1901, 2019.
[93] A. Anuchin, et al., "Adaptive efficient control for switch-reluctance drives with DCDC-regulator for inverter supply," EPE Power Electronics and Motion Control Conference, pp. 1–5, 2004.
[94] A. Anuchin, V. Kozachenko, "Current loop dead-beat control with the digital PI-controller." Eur. Conf. Power Electron. Appl., pp. 1–8, 2014.
[95] A. Dianov and S.T. Lee, "Novel IPMSM drive for compact washing machine," in Proc. 31st Int. Telecommun. Energy Conf., 2009, pp. 1–7.
[96] A. Dianov, "Improved field-weakening control of PM motors for home appliances excluding speed loop windup," IEEE/ASME Trans. Mechatronics, vol. 30, no. 6, pp. 5110-5119, Dec. 2025.
[97] D. Zhao, et al., "Control of an ultrahigh-speed centrifugal compressor for the air management of fuel cell systems," IEEE Trans. Ind. Appl., vol. 50, no. 3, pp. 2225-2234, May/Jun. 2014.
[98] W. Xu, et al., "Reference and limit governors for limit protection of turbofan engines," Energies, 12, 2803, pp. 1–18, Jul., 2019.
[99] U.V. Kalabić, et al., "Reference governors for enforcing compressor surge constraints," IEEE Trans. Control Syst. Tech., vol. 24, no. 5, pp. 1729-1739, Sept. 2016.
[100] S.A. Albarri, A. Khalil, S. Mukhopadhyay and H. Rehman, "Electric vehicle traction system performance enhancement using a high-gain adaptive controller," IEEE Access, vol. 12, pp. 95972-95985, 2024.
[101] W. Uddin et al., "Enhancing the active and reactive power quality of doubly fed induction generator using adaptive PI controller," Int. Conf. Power Generation Syst. Renewable Energy Tech., 2018, pp. 1-6.
[102] A. Dianov and A. Anuchin, "Phase loss detection using voltage signals and motor models: A review", IEEE Sensors Journal, vol. 21, no. 23, pp. 26488-26502, Dec., 2021
[103] A. Dianov, "Stoppage noise reduction of reciprocating compressors," IEEE Trans. on Ind. Appl., vol. 57, no. 5, pp. 4376-4384, Sept./Oct. 2021.
[104] A. Dianov, "Inverter temperature monitoring of cordless tool motor drives." IEEE Open J. of the Ind. Electron. Soc., vol. 4, pp. 52-62, 2023.
[105] H.D. Do, et al., "Overvoltage protection for interior permanent magnet synchronous motor test bench." Int. Workshop on Electric Drives: Optimization in Control of Electric Drives, pp. 1–5, 2017.
[106] A. Dianov, "A novel phase loss detection method for low-cost motor drives." IEEE Trans. Power Electron., vol. 37, no. 6, pp. 6660-6668, Jun. 2022.

ANTON DIANOV (Senior Member, IEEE) received the BSc(hns.), MSc(hns.), and PhD degrees in electrical engineering from the National Research University "Moscow Power Engineering Institute", Moscow, Russia, in 2000, 2002, and 2005, respectively.
From 2005 to 2021, he was a Senior Engineer with Samsung Electronics, where he developed motor drives for home appliances. His research interests include electrical drives, sensorless, and advanced control algorithms. He is the author of several patents and more than 60 refereed publications in his areas of interest. He is an Associate Editor for IEEE OPEN JOURNAL OF THE INDUSTRIAL ELECTRONICS SOCIETY and IEEE JOURNAL OF EMERGING AND SELECTED TOPICS IN POWER ELECTRONICS. Dr. Dianov was awarded with personal scholarships form the President of Russian Federation. He was the recipient of the Wenzhou Ouyue outstanding high talent award.

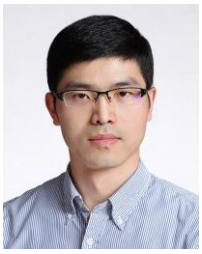

XIAODONG SUN (Senior Member, IEEE) received the B.Sc. degree in electrical engineering, and the M.Sc. and Ph.D. degrees in control engineering from Jiangsu University, Zhenjiang, China, in 2004, 2008, and 2011, respectively.
He has been with Jiangsu University since 2004 and is currently a Professor of Vehicle Engineering at the Automotive Engineering Research Institute. His research interests include electrified vehicles, electrical machines and drives, and energy management. He has authored or coauthored over 100 refereed papers, one book, and holds 42 patents. Dr. Sun is an Associate Editor of the IEEE TRANSACTIONS ON INDUSTRIAL ELECTRONICS, and IEEE TRANSACTIONS ON TRANSPORTATION ELECTRIFICATION.

JIAWEI XIANG (Senior Member, IEEE) (SM'2023) received the B.Sc. degree in mechatronics from Hunan University, China, in 1997, the M.Sc. and PhD degrees in mechanical engineering from Guangxi University, China, in 2003, and from Xi'an Jiaotong University, China, in 2006, respectively. He is currently a professor at the College of Mechanical and Electrical Engineering, Wenzhou University, China. His research interests are the condition monitoring of mechanical systems, structural health monitoring, numerical simulation, signal processing, and vibration analysis. He is also a Fellow of IET, Executive director of the Chinese Society of Vibration Engineering (CSVE), and a member of ASME.

YURIY VAGAPOV received the Dip. Eng. and Ph.D. degrees from Nizhny Novgorod State Technical University, Nizhny Novgorod, Russia, in 1982 and 1995 respectively. He is a Reader in Electrical Engineering at Glyndwr University, Wrexham, Wales, U.K. His academic interests are in the area of electrical engineering specifically power electronics, electrical machines and drives, and electric vehicles. He is a Chartered Engineer and member of the IET.